

Los Alamos National Laboratory is operated by the University of California for the United States Department of Energy under contract W-7405-ENG-36

NOV 08 1985

TITLE SINGLE PARTICLE FEL EQUATIONS WITH OVERTONES

AUTHOR(S) C. J. Elliott and M J. Schmitt

LA-UR--85-3862

DE86 002423

SUBMITTED TO For Publication in Proceedings of Seventh International Free Electron Laser Conference, Tahoe City, NV, September 8-13, 1985.

DISCLAIMER

This report was prepared as an account of work sponsored by an agency of the United States Government. Neither the United States Government nor any agency thereof, nor any of their employees, makes any warranty, express or implied, or assumes any legal liability or responsibility for the accuracy, completeness, or usefulness of any information, apparatus, product, or process disclosed, or represents that its use would not infringe privately owned rights. Reference herein to any specific commercial product, process, or service by trade name, trademark, manufacturer, or otherwise does not necessarily constitute or imply its endorsement, recommendation, or favoring by the United States Government or any agency thereof. The views and opinions of authors expressed herein do not necessarily state or reflect those of the United States Government or any agency thereof.

By acceptance of this article, the publisher recognizes that the U.S. Government retains a nonexclusive, royalty-free license to publish or reproduce the published form of this contribution, or to allow others to do so, for U.S. Government purposes.

The Los Alamos National Laboratory requests that the publisher identify this article as work performed under the auspices of the U.S. Department of Energy.

MASTER
Los Alamos Los Alamos National Laboratory
Los Alamos, New Mexico 87545

FORM NO 838 84
BT NO 2629 5/81

DISTRIBUTION OF THIS DOCUMENT IS UNLIMITED

Single Particle FEL Equations with Overtones

C.J. Elliott and M.J. Schmitt
Los Alamos National Laboratory
University of California
X-1,E531
Los Alamos, NM 87545

Abstract

We report a generalization of the usual single-particle equations for a linear polarized wiggler. Particle simulations show the presence of harmonics under conditions of low γ and high magnetic fields. These harmonics are introduced into the single particle equations by separate field components for each harmonic. The overtones are fed by the same phase space and all their effects on the particle motion are treated simultaneously. The coupling of the magnetic field differs from the usual Bessel function form because of the low electron energy and the high magnetic field. We also include longitudinal space charge fields. We compare the reduced equation results with a full 1D particle simulation. Finding good agreement, we conclude that harmonic generation has a significant impact on the waveform under these conditions.

1. Introduction

Our theoretical description of a planar FEL (free-electron laser) begins with a 1D3V (one distance, three velocities) simulation of Maxwell's equations and the Lorentz force equation, it ends with a reduced description that may be regarded as a generalization of the usual single particle description. This work is still in progress. The boundary conditions used in the simulation are periodic in the dimension coordinate that plays the role of a phase in the reduced description. This reduced description permits time steps that are an order of magnitude larger than that used in the simulation, the number of particles was two orders of magnitude less, and the equations are simpler and more amenable to interpretation.

The periodic grid assumption of the simulation permits motion of the e-beam to occur. The grid is fixed in space but may be thought of as periodically extended *ad infinitum* to the right. In time the electrons move at relativistic speeds to the right. The optical pulse moves faster to the right but also is periodic. On the extended grid, if our eye were fixed on a single particle, it would follow it continually to the right. Equivalently, we could watch the motion within a sole period and as the particle moved out of the right boundary we would see its equivalent enter the left. We use the economy of this one period description in particle simulations where the period is chosen to be a multiple of both the optical

wavelength and the wiggler wavelength.

The reduced description path is to average the contribution to each harmonic as the electrons slip back one optical wavelength. The fundamental optical frequency component is a sinusoidal waveform with phase varying from 0 to 2π . Suppose a source were to give more energy to the phase at $\pi/2$ than to $3\pi/2$, then it would distort the waveform by exciting overtones. To complete the description we consider each harmonic amplitude separately and sum those contributions at $\pi/2$ and $3\pi/2$, among others, weighted by the harmonic phasor. In performing the averaging, we obtain a coupling coefficient that differs from that of Colson[2], Madey and Taber[3], and McNeil and Firth[4,5].

2. Mathematical Description

2.1 1D Maxwell Equations

First we describe the equations used in our WAVE simulation. They originate from those in the chapter *Fundamentals of Particle Simulation*, described by D. Forslund[1]; but they are modified in two respects. First we use charge neutralization, with the average density $\langle \rho \rangle$ subtracted out, and second we use only the time rate of change of the transverse part of the coulomb gauge vector potential \vec{A} to determine the electric field. The latter operation makes the results of the code stable to unphysical and unmathematical temporal drifts in the longitudinal part of \vec{A} and corresponds to voltage-short boundary conditions across the grid. The former condition is required mathematically with periodic boundary conditions and corresponds to achievable physical conditions; eg. at physical beam center.

The quantities we use are in standard notation. The vector \vec{e}_1 is a unit vector in the longitudinal direction. The scalar potential ϕ and the vector potential \vec{A} give the electric and magnetic fields \vec{E} and \vec{B} . The electron has charge of magnitude e and rest mass m with the ratio of the mass to rest mass designated γ . Here ρ is the charge density and \vec{J}_w is a virtual current that produces the static wiggler field.

Maxwell's equations are:

$$\partial_1^2 \vec{A} - \partial_1^2 \vec{A} = \vec{e}_1 \partial_1 \dot{\phi} - \vec{J}_e,$$

$$\partial_1^2 \dot{\phi} = \partial_1 J_{e1},$$

$$\partial_1^2 \phi = \rho - \langle \rho \rangle,$$

$$\dot{A}(L) = \dot{A}(0),$$

$$\dot{\phi}(L) = \dot{\phi}(0),$$

$$\phi(L) = \phi(0),$$

$$\partial_1 A_1 = 0,$$

Here L is the periodic boundary condition length, chosen to be the wiggler wavelength $\lambda_w = 2\pi/k_w$ in the simulations. Also

$$\vec{E} = -\vec{e}_1 \partial_1 \phi - \partial_t (\vec{e}_1 \times \vec{A}) \times \vec{e}_1,$$

$$\vec{B} = \partial_1 (\vec{e}_1 \times \vec{A}).$$

These are coupled to the particle equations by;

$$d_t m \gamma \vec{v} = -e(\vec{E} + \vec{v} \times \vec{B}),$$

$$d_t x_1 = v_1,$$

$$\vec{J}_c = \rho \vec{v} + \vec{J}_w,$$

$$\vec{J}_w = \vec{e}_2 a_k k_w^2 \sin(k_w x_1).$$

The convention here is using *sin* in \vec{J}_w rather than the *cos* convention we use in the reduced equations as does ref. [2].

2.2 Reduced Equations

Derivation of the reduced equations follows ref. [2] with an important modification to the coupling coefficient, a more complete resonant condition, and a sum over harmonics. The standard Madey and Taber[3] coupling coefficient that Colson derives without typographical error is based upon the fourier transform arising from the axial location that varies as $\sin(2\omega_0 t)$, or $\sin(2k_w x_1)$. An incomplete description of a correction to this coupling coefficient has been submitted as ref. [4,5] based upon the change in the axial component of the electron velocity rather than that to the total energy. Our approach is different, it includes treatment of the exact motion of an electron that has all even harmonics of $k_w x_1$ present, and we fourier transform an elliptical integral function phasor to find the coupling coefficient, but do not include terms arising from non-exponential multiplicative variations via dt/dx_1 . Our approach considers a 1D description in γ and phase ζ of the particle and does not lead to the ref. [4,5] corrections. In fact, rather than resulting in an enhancement of the fundamental, our correction reduces to the Madey-Taber-Colson coefficient at high γ . At low γ (and high magnetic field) when our correction is important, it decreases the coupling of the fundamental rather than giving the ref. [4,5] enhancement. When we write the expression for $\dot{\gamma}$ in terms of $\dot{\beta}_1$ we find additional terms that just cancel the ref. [4,5] $1/f$ terms and thereby give the Madey-Taber-Colson result at large γ .

2.2.1 The Coupling Coefficient

The coupling coefficient is derived mathematically by expanding the expression

$$cc = \cos(k_w x_1) \cos(k_w x_1 - \omega_e t + \phi) \beta c \frac{dt}{dx_1},$$

using an elliptical integral expression for $t(x_1)$, the time an electron reaches location x_1 , and $c\beta$ is the average velocity in the x_1 direction. In the calculations reported here we drop the $\beta c(dt/dx_1)$ in lieu of the expected rapid variation of the phase term. Here we

take $\omega_s = k_s c$. The time $t(x_1)$ can be represented by the sum of a term linear in x_1 and a term doubly periodic in x_1 . The linear term combines with k_w and k_s to form the resonant condition. The periodic term can be expanded in a fourier series in the even harmonics of $k_w x_1$. These ideas produce the mathematical identity

$$cc = \frac{1}{2} \sum_{-\infty}^{\infty} (c_n + c_{n+1}) \cos[k_s(1 - \bar{\beta}^{-1})x_1 + (2n+1)k_w x_1 + \phi],$$

with the resonant condition obtained when the \cos argument is stationary with respect to x_1 , and where we regard the parameters a_k, γ and k_w as constants and start with

$$t(x_1) = \int_0^{x_1} \frac{dx_1}{[c^2(1 - \gamma^{-2}) - c^2 a_k^2 \gamma^{-2} \cos^2 k_w x_1]^{1/2}},$$

and end with

$$c_n = \frac{1}{\pi} \int_0^{\pi} \cos[\Phi(\theta/2) + n\theta] \bar{\beta} c \frac{dt}{dx_1} d\theta,$$

where for the numerical and analytical work here the $\bar{\beta} c(dt/dx_1)$ term has been replaced by unity. Above, the function Φ is given by

$$\Phi(A) = \frac{k_s}{k_w(1 - \gamma^{-2})^{1/2}} \left[F\left(\frac{\pi}{2} + A|m\right) - F\left(\frac{\pi}{2}|m\right) \left(1 + \frac{2A}{\pi}\right) \right].$$

The quantities β and m are

$$\bar{\beta} = \frac{\pi(1 - \gamma^{-2})^{1/2}}{2F\left(\frac{\pi}{2}|m\right)},$$

and

$$m = \frac{a_k^2}{\gamma^2 - 1},$$

where F is the elliptical integral of the first kind defined in the *Handbook of Mathematical Functions*[6] by (17.2.6). A special case that occurs for small m , evaluated at the harmonic resonance gives the Madey-Taber-Colson result at high γ

$$\Phi(\theta) \xrightarrow{m \rightarrow 0} \frac{(2n+1)m}{8(1 - \beta)(1 + \frac{m}{4})} \sin 2\theta \xrightarrow{\gamma \rightarrow \infty} \frac{a_k^2 \sin 2\theta}{4 + 2a_k^2},$$

$$\bar{\beta} \xrightarrow{m \rightarrow 0} \frac{(1 - \gamma^{-2})^{1/2}}{1 + \frac{m}{4}} \xrightarrow{\gamma \rightarrow \infty} 1 - \frac{1}{2\gamma^2} \left(1 + \frac{a_k^2}{2}\right),$$

and

$$c_n \xrightarrow{m \rightarrow 0} J_n \left[\frac{(2n+1)m}{8(1 - \beta)(1 + \frac{m}{4})} \right] \xrightarrow{\gamma \rightarrow \infty} J_n \left[\frac{(2n+1)a_k^2}{4 + 2a_k^2} \right].$$

A physical interpretation of the coupling coefficient identity is that the harmonics in the $t(z)$ motion produce an effectively higher harmonic wiggler field. That is, if we think of a prototypical linear wiggler as having a single resonance frequency with 100% coupling just as a helical wiggler does, we can view the cc identity as saying that an actual linear wiggler is, on average, a prototypical wiggler having a magnetic field that is a superposition of fields with wave numbers that are the odd harmonics of k_w . The amplitude of the $2n + 1$ harmonic of the effective magnetic field is then just the factor $c_n + c_{n+1}$ multiplied by the actual fundamental field.

2.2.2 Coupling in the Particle Equations

The reduced equations describe the time dependence of the electromagnetic wave by a superposition of the odd harmonics. The WAVE results reported in Section 3 show a consistent time dependence because a uniform e-beam was injected and because the λ_w period for L was chosen. Were one to describe a problem where the local spectral width was small but finite compared to the harmonic separation, he could do so by generalizing the approach of ref. [2] along the lines reported here. Such a case would model a time dependent injected current, for instance.

The electric field is taken to be a superposition of harmonics; allowing only resonant interactions that occur for the l 'th wave vector given by

$$k_{sl} = (2l + 1)k_s \approx \frac{(2l + 1)k_w}{\beta^{-1} - 1},$$

we have

$$\frac{d\gamma}{dt} \approx \sum_{l=0}^{\infty} (c_l + c_{l+1}) e_l \frac{a_k}{2\gamma} \cos|k_{sl}(1 - \beta^{-1})x_1 + (2l + 1)k_w x_1 + \phi_l|.$$

2.2.3 The Reduced Equation Set

Using complex notation, $\mathcal{E}_l = e_l \exp i\phi_l$, we have the square pulse equations,

$$\frac{d\gamma}{d\tau} = \Re \frac{(c_l + c_{l+1})}{2} \mathcal{E}_l \frac{a_k}{\gamma} \exp i(2l + 1)\phi - \frac{eE_1\beta_1}{m_0c^2k_s},$$

$$\frac{d\phi}{d\tau} = \left(1 + \frac{k_w}{k_s}\right) \beta^{-1},$$

$$\frac{d\mathcal{E}_l}{d\tau} = \sum_l \frac{a_k}{2} \rho(c_l + c_{l+1}) \left\langle \frac{\exp -i(2l + 1)\hat{\phi}}{\gamma} \right\rangle.$$

Here, we have taken the propagating wave to be planar, and ρ represents the average electron density in the wiggler measured in ω_p^2/ω_s^2 units; \Re indicates the real part of the expression. The electrostatic term follows reference 2. In its implementation, numerical

noise problems are avoided by subtracting out the initial density vector from the density vector just before integration of \mathcal{L}_1 . The conservation of energy within a computational box follows mathematically from the above equations with $\hat{\phi} = \phi$ and is expressed as

$$\rho \langle \gamma \rangle + \sum_l |\mathcal{E}_l|^2 = \text{constant}.$$

That is, the loss of electron energy density is compensated by the gain in energy density on one or more of the harmonics.

3. Computational Results

3.1 Wave Results

The WAVE particle simulations used 10000 particles with 188 cells in x_1 ranging from 0 to 12π . In this work $k_s/k_w = 6.0$, $\beta_1\gamma = 3.775$ at injection just outside and also just inside the wiggler, $\tau_1 = 47.34$ where τ_1 is the injection time; also we have $\bar{\beta} = 12\pi/\tau_1$; the scaled density is $(\omega_p^2/\omega_s^2)_o = 8.7 \cdot 10^{-6}$ outside the wiggler and $\bar{\beta}^{-1}$ times larger inside. The scaled vector potential magnetic field is $a_k = 2.82$. We used 70000 time steps of $\Delta t = 0.15$. At the fundamental frequency, the shape factor of ref. [7] is $S_1 = 0.9985$, indicating more than adequate spatial resolution. The first run shown in Fig. 1 had magnetic permeability of unity; all other runs had $\mu = 0.99893$. All runs reported here were started from noise.

Simple charge/current neutralization and propagation in free space did not give adequate representation of the expected results. Fig. 1 shows a plot of the optical field energy and magnetic field energy averaged over the computational grid. These results show a drift in the electric field energy at long times that arises from a small non-physical time dependent A_1 component, before the second modification was made to Maxwell's equations. Also the rapid oscillation at $T < 2000$ is attributed to a generated diamagnetic field that slightly altered the presumed equilibrium between the initialized static magnetic field and the initialized virtual current.

The calculation shown in Fig. 2 shows similar quantities but here the above mentioned problems do not appear. The electrical energy growth rate $\gamma = 0.0055$ in the code units differs substantially from 0.0043 of Fig. 1.

The final wave form of the x_2 component of the electric field is shown in Fig. 3 along with a harmonic decomposition. The significant components are the 1'st, 3'rd, and 5'th harmonics of the fundamental frequency. Theoretical considerations suggest that these components propagate to the right.

The electrons are shown in the $\beta_1\gamma, x_1$ phase space in Fig. 4a and their density in Fig. 4b. We can clearly see the bunching occurring in both figures. Most of the variation in the density peak amplitude is attributed to the variation of β_1 , but the peaks are not equally separated in time or space.

3.2 Reduced Equation Calculations

The coupling coefficient for the fundamental frequency that is used in the reduced equations is shown in Fig. 5. It differs substantially from a variation of 0.755 to 0.745 that occurs by

approximating Φ by a $\sin 2k_w z$ approximation, sans resonance assumption, over the same range, but yet at high γ the two results agree with each other.

The magnitude of the total electrical field is shown in Fig. 6a in the same time units as the WAVE calculation. The harmonics are shown in Fig. 6b. These harmonics are plotted on a time and magnitude scale that requires the subplot to be blown up to the full grid size to read the values. As in the simulation, the harmonics are seen to be appreciable. Here the 100 particles were placed on the grid with equal spacing but then each particle was displaced a small random amount that reproduced the expected noise on the fundamental for 10000 completely randomized particles. This gives more noise on the harmonics than a complete randomization of 10000 particles would give, but may be thought of as being representative of some realizations of 10000 random particles.

The growth rate for this case was computed by finding the largest growth root in solving the cubic equation that arises in the small signal limit of these equations. This small signal theory was used as a means of checking the reduced equation description, giving overlaying plots for the cases compared. The growth rate was 0.00553 in good agreement with 0.0055 from WAVE. This comparison was serendipitous for several reasons: (1) the harmonic modes contribute an undetermined amount to the growth rate in the WAVE case (2) the $\bar{\beta} dt/dx_1$ term may alter the coupling coefficient; (3) the reduced description may be slightly more complicated than that shown.

Acknowledgements

K. Lee suggested attacking the problem of low γ and high a_k by using WAVE. D. Forslund generously answered many questions about modifications to conventions in WAVE. This work was supported by the U.S. Department of Energy.

References

- [1] D. Forslund, *Fundamentals of Particle Simulation*, in *Space Plasma Simulations*, M. Ashour-Abdalla and D. A. Dutton, Eds., Dordrecht: D. Reidel Publishing Company, 1985; also to appear in *Space Science Review*, 1985.
- [2] W. B. Colson, "The nonlinear wave equation for higher harmonics in free-electron lasers," *IEEE J. of Quantum Electron.*, vol. QE-17, pp. 1417-1427, 1981.
- [3] J.M.J. Madey and R.C. Taber, "Equations of motion for a free-electron laser with a transverse gradient," in *Physics of Quantum Electronics*, vol. 7, Jacobs *et al.*, Eds., Reading, MA: Addison-Wesley, 1980, ch. 30.
- [4] B.W.J. McNeil and W.J. Firth, "Effect of the radiation force on free-electron laser gain," *IEEE J. Quantum Electron.*, vol. QE-21, pp. 1034-1036, 1985.
- [5] B.W.J. McNeil and W.J. Firth, "Effect of the radiation force on free-electron laser," *Proceedings of this conference*
- [6] *Handbook of Mathematical Functions*, M. Abramowitz and I. Stegun, Eds., Washington DC: US Government Printing Office, 1964, ch. 17.2.6.
- [7] C.K. Birdsall and A.B. Langdon, *Plasma Physics Via Computer Simulation*, New York NY: McGraw-Hill Book Company, 1985, ch. 4.6.

ROUGH DRAFT

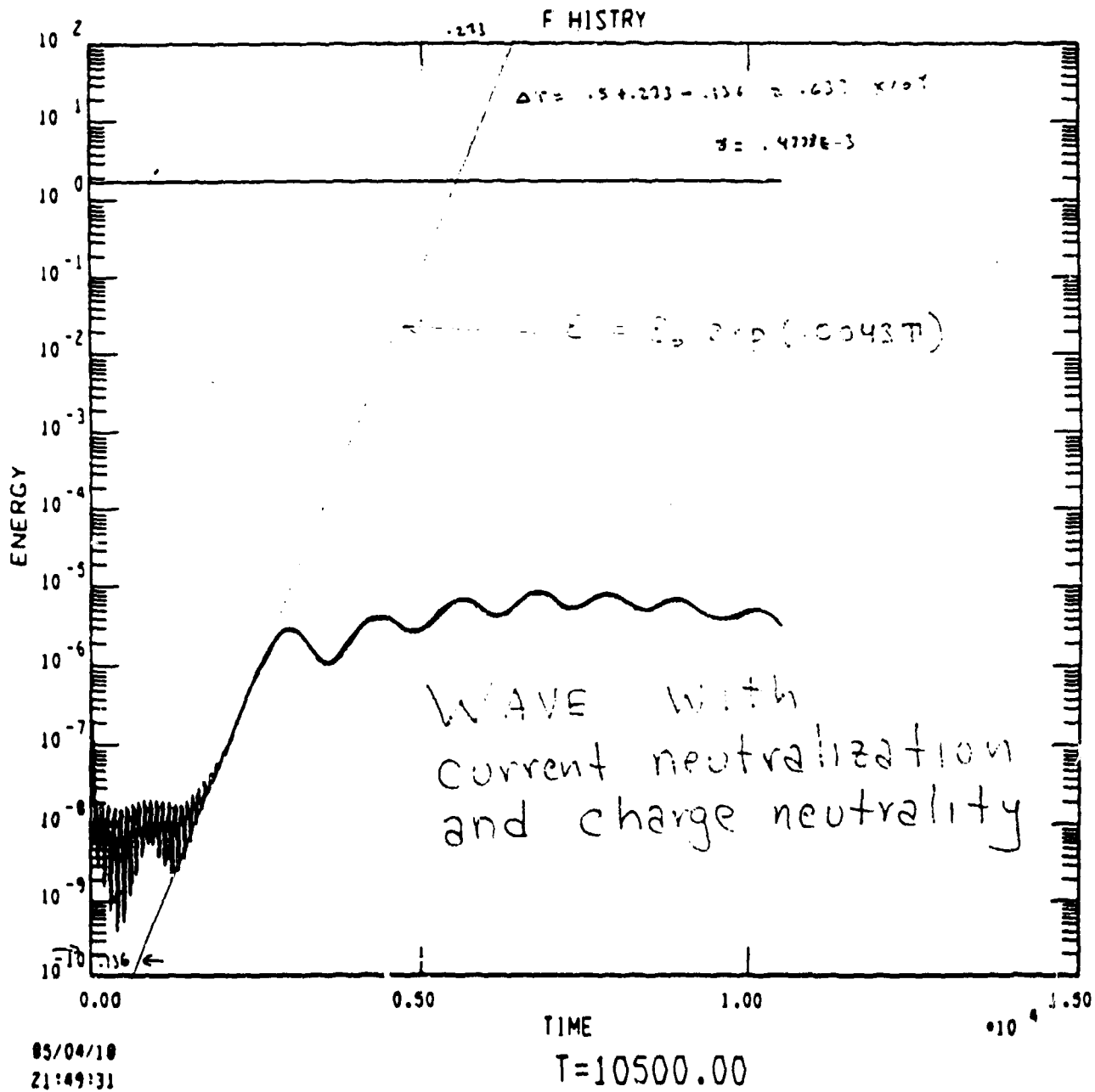


Fig. 1 WAVE plot of energy of field versus time. The drift in the synchrotron bumps is caused by $\partial_t A_1$ and initial oscillations are caused by a diamagnetic effect. The upper line is the total magnetic field energy, the lower line the total electric field energy. Fit to the straight line portion of the lower curve gives $energy = \epsilon_0 \exp(.0043T)$.

ROUGH DRAFT

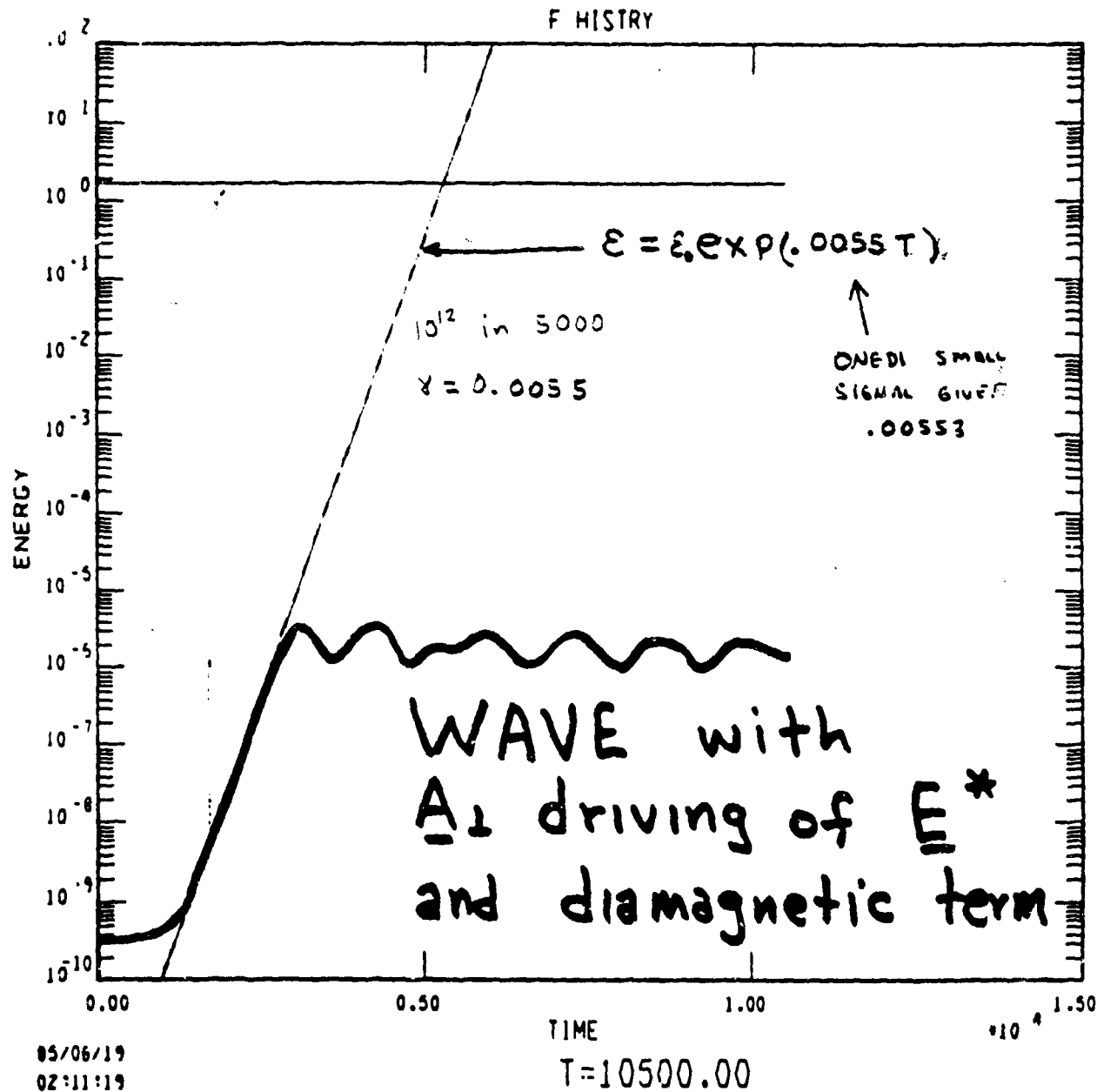


Fig. 2 Wave plot of energy versus time as in Fig. 1. Diamagnetic oscillations do not appear. Removal of the $\partial_t A_1$ term has accounts for the lack of drift in the synchrotron bumps. Fit to the straight portion of the lower curve gives $energy = \epsilon_0 \exp(.0055T)$.

ROUGH DRAFT

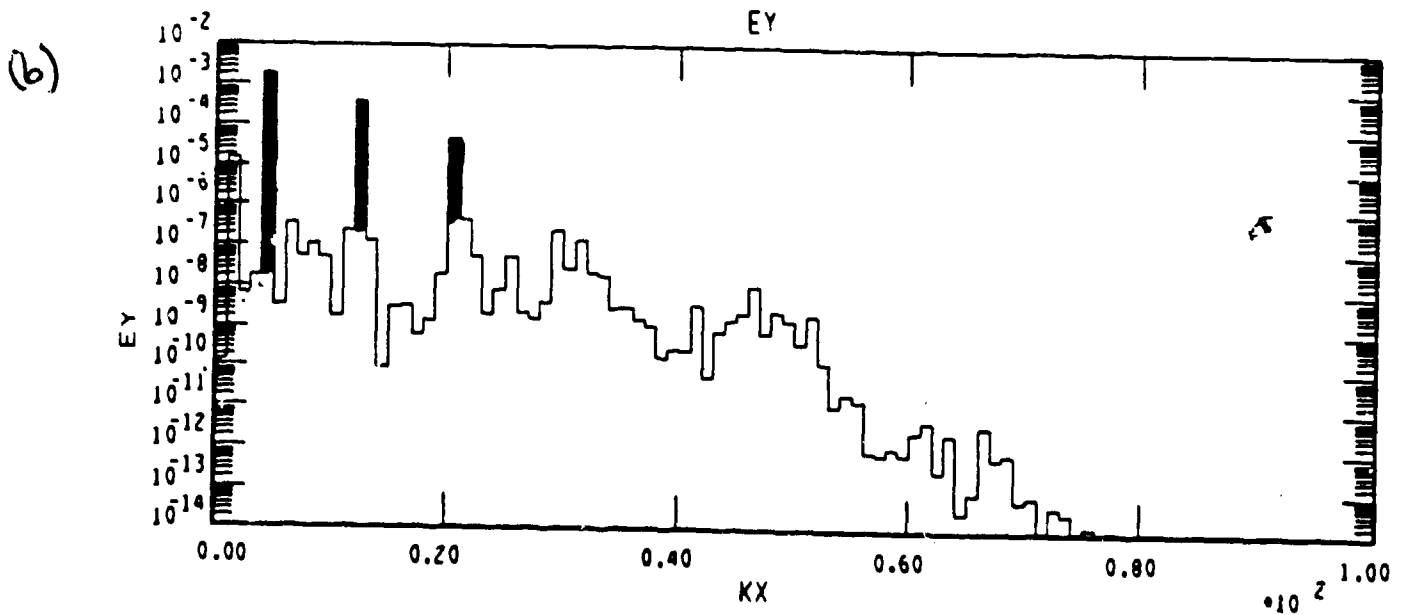
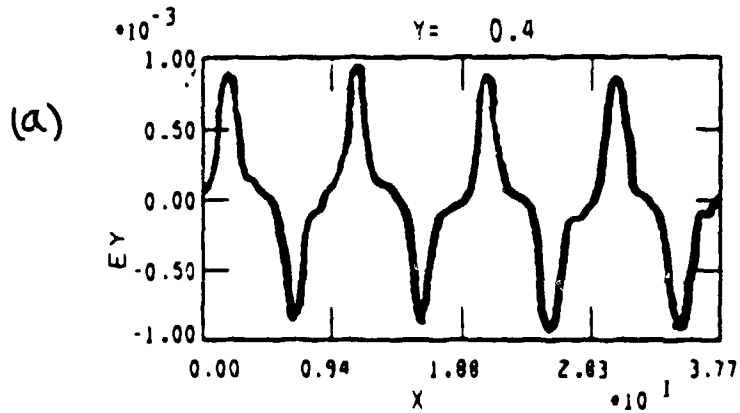


Fig. 3 Waveform and harmonic decomposition of the propagating field $E_y = E_2$ at time $T = 10500$.

ROUGH DRAFT

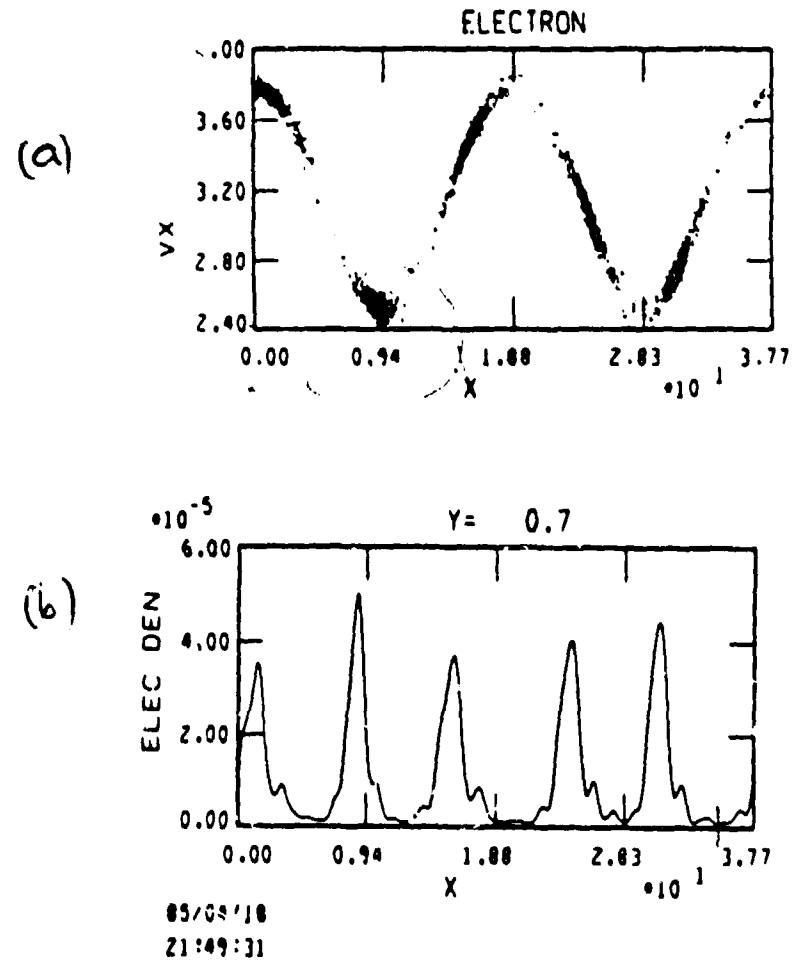


Fig. 4 (a) The $(\beta_1 \gamma, x_1)$ phase space plot of the electrons at time $T = 10500$.
(b) The density corresponding to the phase space plot.

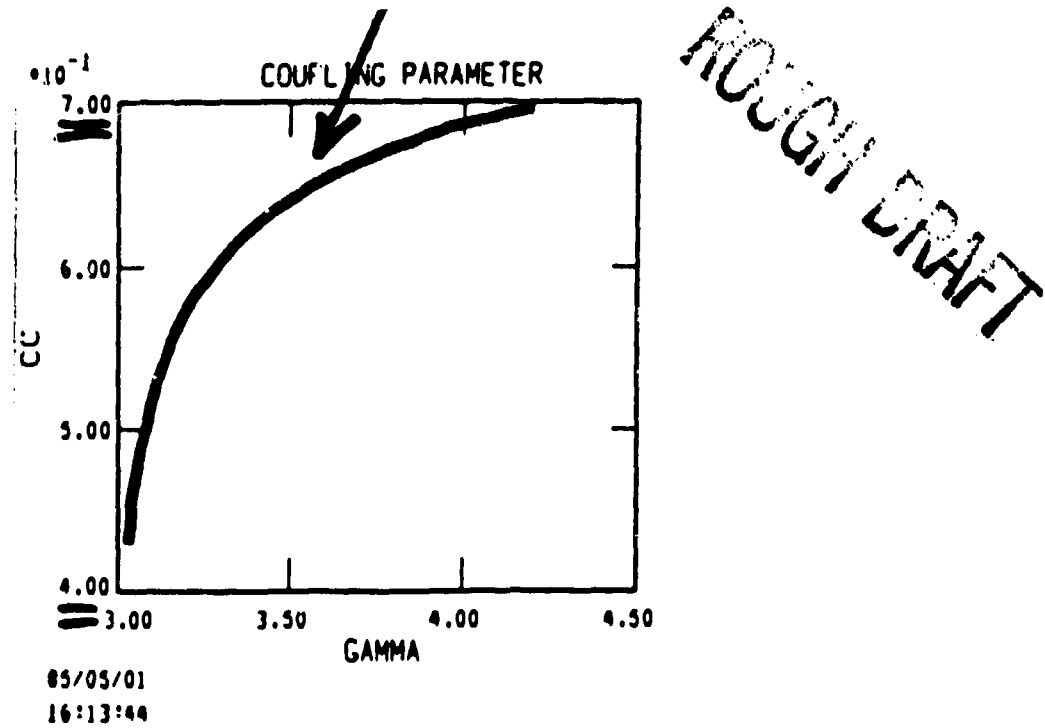


Fig. 5 The coupling parameter $c_0 + c_1$ versus γ for the conditions of the calculation.

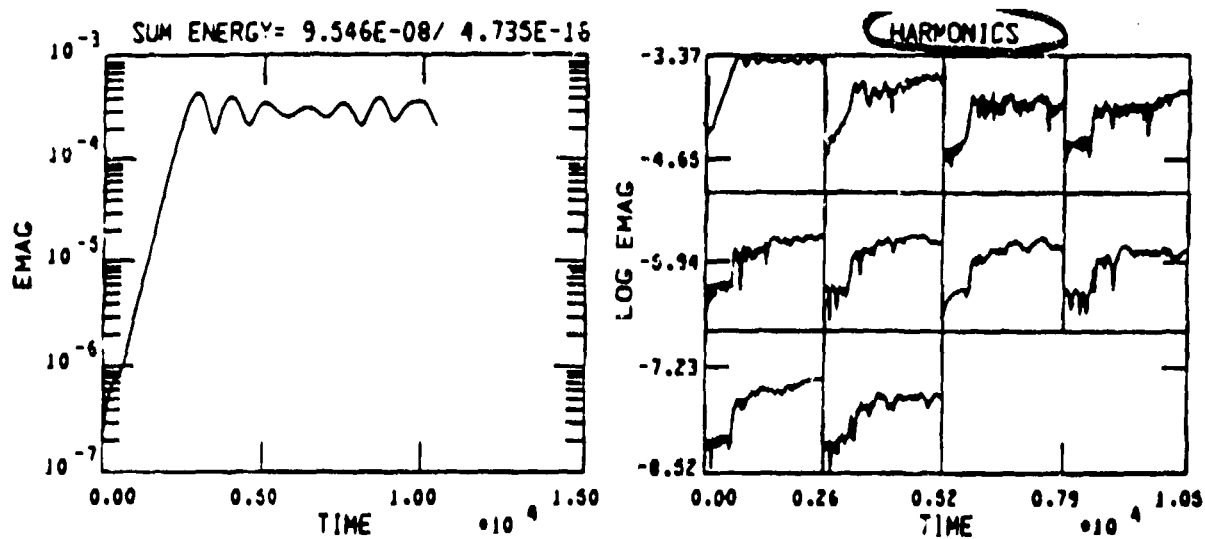


Fig. 6 (a) $\sum |e_l|^2$ in the reduced equations starting from noise. Compare to Fig. 2. (b) The 1'st, 3'rd, 5'th, ...19'th harmonic fields versus time, appearing as one reads. To use the scale, the subplot is expanded to fit the labeled axes. The first subplot repeats (a).